Synthesis and Structural Characterization of Low-Valent Group V Phosphine Complexes

John D. Protasiewicz, Patricia A. Bianconi, Ian D. Williams, Shuncheng Liu, Ch. Pulla Rao, and Stephen J. Lippard*

Department of Chemistry, Massachusetts Institute of Technology, Cambridge, Massachusetts 02139

Received March 25, 1992

The compounds $[Nb(CO)_2(dmpe)_2Cl]$ and $[Ta(CO)_2(dmpe)_2Cl]$, where dmpe = 1,2-bis(dimethylphosphino)ethane, are important precursors in chemistry leading to the reductive coupling of carbon monoxide ligands to form bis(trialkylsiloxy)acetylenes. Convenient, high-yield syntheses of these seven-coordinate niobium(I) and tantalum(I) complexes have been devised by utilizing catalytic Mg(anthracene) to reduce either $[NbCl_4(dmpe)_2]$ or $[TaCl_4(dmpe)_2]$ under an atmosphere of CO. With the use of Mg(anthracene)·3THF in the absence of CO, the complexes $[TaCl_2(dmpe)_2]$ (**1**) and $[Ta(\eta^4\text{-anthracene})(dmpe)_2Cl]$ (**2**) were obtained, both of which have been structurally characterized by X-ray crystallography. The preparation of $[V(CO)_2(dmpe)_2Me]$ and the crystal structure determinations of several related seven-coordinate $[M(CO)_2(dmpe)_2X]$ complexes (M = V, X = Me (**8**); M = Nb, X = Cl (**4**), I (**5**); M = Ta, X = Me (**7**)) and $[Ta(CO)_2(depe)_2Cl]$ (**6**), depe = 1,2-bis(diethylphosphino)ethane, having the capped trigonal prismatic geometry, are also described. These complexes all have acute OC-M-CO angles, low ν_{CO} stretching frequencies, and close nonbonded C···C contacts, features which indicate their propensity to undergo reductive coupling reactions. The alkyl complexes $[V(CO)_2(dmpe)_2Me]$ and $[Ta(CO)_2(dmpe)_2Me]$ display abnormally long M-C σ bond lengths, 2.31 (1) and 2.32 (1) Å, respectively. Crystal data: (**1**) monoclinic, $P2_1/n$, a = 9.384 (1) Å, b = 12.863 (2) Å, c = 9.363 (1) Å, β = 95.04 (1)°, Z = 2, R = 0.030, R_w = 0.039; (**2**) triclinic, $P\bar{1}$, a = 12.997 (6) Å, b = 13.495 (3) Å, c = 18.860 (4) Å, α = 75.38 (2)°, β = 84.75 (5)°, γ = 89.50 (5)°, Z = 4, R = 0.043, R_w = 0.063; (**4**) orthorhombic, $Pna2_1$, a = 16.106 (3) Å, b = 8.333 (1) Å, c = 33.881 (5) Å, Z = 8, R = 0.045, R_w = 0.060; (**5**) orthorhombic, $Pnma$, a = 16.571 (2) Å, b = 16.632 (2) Å, c = 8.439 (1) Å, Z = 4, R = 0.038, R_w = 0.046; (**6**) triclinic, $P\bar{1}$, a = 11.245 (1) Å, b = 13.325 (2) Å, c = 10.881 (2) Å, α = 99.58 (1)°, β = 112.44 (1)°, γ = 70.24 (1)°, Z = 2, R = 0.018, R_w = 0.023; (**7**) orthorhombic, $Fdd2$, a = 10.615 (1) Å, b = 33.123 (7) Å, c = 12.766 (2) Å, Z = 8, R = 0.029, R_w = 0.037; (**8**) orthorhombic, $P2_12_12_1$, a = 13.509 (3) Å, b = 13.777 (2) Å, c = 11.719 (2) Å, Z = 4, R = 0.050, R_w = 0.055.

Introduction

The chemistry of the group V transition metals in their lower oxidation states has been a subject of considerable recent interest.[1-3] The reductive coupling of nitriles,[4,5] isocyanides,[6-8] and carbon monoxide,[9,10] the activation of alkynes,[11-20] and the synthesis and characterization of dinitrogen complexes[21-25] and polyhydrides[26-29] have all been reported for low-valent group V complexes.

The work presented here was carried out as an integral part of our ongoing program to investigate reductive coupling reactions in group V carbonyl and group VI isocyanide complexes.[9,30] Specifically, we sought synthetic routes to M(I) dicarbonyl complexes with good σ donor ligands in accord with the electronic and geometric requirements thought to promote reductive coupling of isocyanide or carbon monoxide ligands.[31,32] Here we describe improved preparations of $[Ta(CO)_2(dmpe)_2Cl]$ and $[Nb(CO)_2(dmpe)_2Cl]$, important precursors for the reductive coupling of two CO ligands and the cross coupling of CO and CNR ligands.[7,9,30,33] The niobium complex was structurally characterized, as were four other geometrically related seven-coordinate species, $[Nb(CO)_2(dmpe)_2I]$, $[Ta(CO)_2(depe)_2Cl]$, $[Ta(CO)_2(dmpe)_2Me]$, and $[V(CO)_2(dmpe)_2Me]$. During an attempted synthesis of $[Ta(CO)_2(dmpe)_2Cl]$ by using Mg(anthracene)·3THF and $[TaCl_4(dmpe)_4]$, an alternative preparation of $[TaCl_2(dmpe)_2]$ was discovered, as well as an interesting tantalum an-

(1) Calderazzo, F.; Pampaloni, G. *J. Organomet. Chem.* **1992**, *423*, 307.
(2) Srivastava, S. C.; Shrimal, A. K. *Polyhedron* **1988**, *7*, 1639.
(3) Ellis, J. E. *Adv. Organometallic Chem.* **1990**, *31*, 1.
(4) Finn, P. A.; King, M. S.; Kilty, P. A.; McCarley, R. E. *J. Am. Chem. Soc.* **1975**, *97*, 220.
(5) Cotton, F. A.; Hall, W. T. *J. Am. Chem. Soc.* **1979**, *101*, 5094.
(6) Carnahan, E. M.; Lippard, S. J. *J. Chem. Soc., Dalton Trans.* **1991**, 699.
(7) Carnahan, E. M.; Lippard, S. J. *J. Am. Chem. Soc.* **1990**, *112*, 3230.
(8) Cotton, F. A.; Roth, W. J. *J. Am. Chem. Soc.* **1983**, *105*, 3734.
(9) Vrtis, R. N.; Lippard, S. J. *Isr. J. Chem.* **1990**, *30*, 331.
(10) Protasiewicz, J. D.; Lippard, S. J. *J. Am. Chem. Soc.* **1991**, *113*, 6564.
(11) Hurtung, J. B., Jr.; Pedersen, S. F. *J. Am. Chem. Soc.* **1989**, *111*, 5468.
(12) Kataoka, Y.; Takai, K.; Oshima, K.; Utimoto, K. *J. Org. Chem.* **1992**, *57*, 1615.
(13) Takai, K.; Tezuka, M.; Kataoka, Y.; Utimoto, K. *J. Org. Chem.* **1990**, *55*, 5310.
(14) Takai, K.; Miyai, J.; Kataoka, Y.; Utimoto, K. *Organometallics* **1990**, *9*, 3030.
(15) Takai, K.; Kataoka, Y.; Utimoto, K. *J. Org. Chem.* **1990**, *55*, 1707.
(16) Kataoka, Y.; Takai, K.; Oshima, K.; Utimoto, K. *Tetrahedron Lett.* **1990**, *31*, 365.
(17) Kataoka, Y.; Miyai, J.; Tezuka, M.; Takai, K. *Tetrahedron Lett.* **1990**, *31*, 369.
(18) Curtis, M. D.; Real, J. *Organometallics* **1985**, *4*, 940.
(19) McGeary, M. J.; Gamble, A. S.; Templeton, J. L. *Organometallics* **1988**, *7*, 271.
(20) Bruck, M. A.; Copenhaver, A. S.; Wigley, D. E. *J. Am. Chem. Soc.* **1987**, *109*, 6525.
(21) Edema, J. J. H.; Meetsma, A.; Gambarotta, S. *J. Am. Chem. Soc.* **1989**, *111*, 6878.
(22) Woitha, C.; Rehder, D. *Angew. Chem., Int. Ed. Eng.* **1990**, *29*, 1438.
(23) Rocklage, S. M.; Schrock, R. R. *J. Am. Chem. Soc.* **1982**, *104*, 3077.
(24) Rocklage, S. M.; Turner, H. W.; Fellmann, J. D.; Schrock, R. R. *Organometallics* **1982**, *1*, 703.
(25) Burt, R. J.; Leigh, G. J. J.; Hughes, D. L. *J. Chem. Soc., Dalton Trans.* **1981**, 793.
(26) Luetkens, M. L.; Huffman, J. C.; Sattelberger, A. P. *J. Am. Chem. Soc.* **1983**, *105*, 4474.
(27) Luetkens, M. L.; Elcesser, W. L.; Huffman, J. C.; Sattelberger, A. P. *Inorg. Chem.* **1984**, *23*, 1718.
(28) Luetkens, M. L.; Huffman, J. C.; Sattelberger, A. P. *J. Am. Chem. Soc.* **1985**, *107*, 3361.
(29) Schrock, R. R. *J. Organomet. Chem.* **1976**, *121*, 373.
(30) Carnahan, E. M.; Lippard, S. J. *J. Am. Chem. Soc.* **1992**, *114*, 4166.
(31) Bianconi, P. A.; Vrtis, R. N.; Rao, C. P.; Williams, I. D.; Engeler, M. P.; Lippard, S. J. *Organometallics* **1987**, *6*, 1968.
(32) Vrtis, R. N.; Bott, S. G.; Rao, C. P.; Liu, S.; Lippard, S. J. *Organometallics* **1991**, *10*, 275.
(33) Datta, S.; Wreford, S. S. *Inorg. Chem.* **1977**, *16*, 1134.

0020-1669/92/1331-4134$03.00/0

thracene complex, [Ta(η^4-anthracene)(dmpe)$_2$Cl]. Single crystal X-ray studies of these two complexes are also reported.

Experimental Section

General Methods. All reactions and manipulations were carried out under a nitrogen atmosphere by using standard Schlenk techniques or a Vacuum Atmospheres drybox. Solvents were distilled under nitrogen from sodium benzophenone ketyl. Deuterated solvents were dried by passage over a column of alumina and stored under nitrogen over molecular sieves. [Mg(anthracene)·3THF],[34] [TaCl$_4$(dmpe)$_2$],[27,33] [NbCl$_4$(THF)$_2$],[35] [NbCl$_4$(dmpe)$_2$],[35] [TaCl$_2$(dmpe)$_2$],[33] and Na[V(CO)$_2$(dmpe)$_2$][10] were synthesized by literature procedures. [Ta(CO)$_2$(dmpe)$_2$Me] was prepared by replacing MeI with MeOTf (OTf = O_3SCF_3) in the original procedure.[33] A sample of 10% enriched ^{13}CO was purchased from Cambridge Isotopes. Proton chemical shifts were referenced to residual solvent peaks. ^{31}P{^{1}H} NMR spectra were recorded on either a JEOL FX90 or Varian XL300 spectrometer and referenced to external phosphoric acid. ^{1}H and ^{13}C{^{1}H} NMR spectra were recorded on Bruker WM250, Bruker WM270, and Varian XL300 instruments. EPR spectra were obtained on a Varian E-line X band spectrometer operating at ~9.4212 GHz. The g values were calibrated with the Mn(II) impurity in strontium oxide (g = 2.0012). Mass spectra were run on a Finnigan MAT 8200 instrument. X-ray diffraction data were collected on an Enraf-Nonius CAD4 diffractometer.

Syntheses. [TaCl$_2$(dmpe)$_2$] (1). A portion of Mg(anthracene)·3THF (0.418 g, 1.0 mmol) was added to a stirred solution of 0.623 g of [TaCl$_4$(dmpe)$_2$] (1.0 mmol) in 30 mL of THF. After 10 min the initial green solution turned red-brown. An EPR spectrum of this solution showed the presence of [TaCl$_2$(dmpe)$_2$][27,33] and no other EPR detectable species. The solution was evaporated to dryness, the residue was extracted with 50 mL of pentane, and the extract was filtered. After the filtrate was reduced to ca. 5 mL in volume it was cooled to −20 °C, and red crystals of **1** formed that were contaminated with crystals of anthracene. Repeated recrystallization did not completely separate **1** from excess anthracene, and a sample of **1** of analytical purity could not be obtained via this synthetic route. EPR (room temperature, THF solution): eight-line pattern, g = 1.955, A = 230 G; lit. (benzene) g = 1.943.

[Ta(η^4-anthracene)(dmpe)$_2$Cl] (2). Solid Mg(anthracene)·3THF (0.314 g, 0.75 mmol) was added to a stirred solution of 0.31 g of [TaCl$_4$(dmpe)$_2$] (0.5 mmol) in 30 mL of THF. The initial green solution turned red-brown after 10 min, indicating the formation of [TaCl$_2$(dmpe)$_2$]. After 8 h the solution was red-yellow. It was then evaporated to dryness, and the residue was dissolved in 1:1 toluene/pentane (5 mL). This solution was applied to an alumina column (3 × 9 cm) that had been poured from 1:1 toluene/pentane, and the column was eluted with 150 mL of this same solvent mixture. The column was then eluted with THF; the orange band was collected and evaporated to dryness. Recrystallization at −20 °C from toluene/pentane gave 0.27 g (78%) of **2**. ^{1}H NMR (270 MHz, CD_2Cl_2) (see Figure 2 for numbering scheme) (δ): 1.41 (PCH_3, br); 1.82 (PCH_2, br); 6.42 (s, H76, H78); 6.93, 7.13 (m, H78–H79, H80–H81). ^{13}C{^{1}H} NMR (67.9 MHz, CD_2Cl_2) (δ): 14.6, 17.6 (s, br, PCH_3), 32.4 (s, br, PCH_2), 61.0 (m, C71–C74); 117.2 (s, C76, C73); 122.3, 125.3 (s, C78–C79, C80–C81); 132.2 (s, C77, C82), 151.8 (s, C75, C84). ^{31}P{^{1}H} NMR (36.6 MHz, THF) (δ): 12.6 (s). Anal. Calcd for $C_{26}H_{42}TaP_4Cl$: C, 44.94; H, 6.09; Cl, 5.10. Found: C, 43.64; H, 5.94; Cl, 4.67. Mass spectrum (FAB$^+$, glycerol): m/e 695 ([^{181}Ta$_1^{35}$Cl$_1^{31}$P$_4^{12}$C$_{26}^1$H$_{42}$]$^+$), 517 ([P − $C_{14}H_{10}$]$^+$).

[Ta(CO)$_2$(dmpe)$_2$Cl] (3). To a catalytic quantity of Mg(anthracene) (0.010 g of anthracene and 1.0 g of Mg dust) was added 9.46 g (15.2 mmol) of [TaCl$_4$(dmpe)$_2$] and 300 mL of THF. The initial blue solution quickly turned red-brown, indicating formation of [TaCl$_2$(dmpe)$_2$]. Carbon monoxide was slowly bubbled through the solution, which was left under an atmosphere of CO for 3 days, during which time it turned orange-yellow. Shorter reaction times diminished the yield of **3**. After 3 days the reaction mixture was transferred to the drybox and filtered slowly through a pad of neutral alumina (6 cm height × 8 cm in diameter). The alumina was washed with THF until the washings were colorless. If the filtrate was brown at this point, it was filtered again through fresh alumina. The combined washings were stripped of solvent in vacuo to give orange microcrystalline **3**. Yield: 8.18 g, 94%. Analytical samples were prepared by recrystallization from toluene/pentane at −20 °C. IR (Nujol): 1810 (vs), 1740 (vs), 1415 (m), 1298 (m), 1297 (m), 1080 (w, br), 943 (s), 933 (s, br), 918 (sh), 890 (s), 865 (m), 730 (s), 703 (s), 645 (s, br) cm^{-1}; lit. (THF solution) ν_{CO} = 1833 (vs), 1756 (s) cm^{-1}.[33] ^{31}P-{^{1}H} NMR (THF, 36.6 MHz) (δ): 24.0 ppm (s); lit. (1:1 toluene/THF) 22.7 ppm (s).[33] Analytical and ^{1}H NMR data were also in agreement with literature values.

^{13}CO-enriched [Ta(CO)$_2$(dmpe)$_2$Cl] was prepared in the same manner except that the [TaCl$_4$(dmpe)$_2$]/Mg(anthracene) mixture was stirred for 3 days under 1 atmosphere of 10% enriched ^{13}CO. Workup as above gave [Ta(*CO)$_2$(dmpe)$_2$Cl] in 50% yield. IR (Nujol): ν(^{13}CO) 1777, 1682 cm^{-1}. ^{13}C{^{1}H} NMR (67.9 MHz, THF/10% $CDCl_3$) (δ): 13.47, 15.36 (s, br, PCH_3), 27.90 (s, PCH_2), 273.5 (s, br, CO).

[Nb(CO)$_2$(dmpe)$_2$Cl] (4). A blue solution of [NbCl$_4$(dmpe)$_2$] was generated by addition of dmpe (5.0 g, 33.33 mmol) to a THF solution of [NbCl$_4$(THF)$_2$] (5.90 g, 15.57 mmol). Use of the same procedure and workup as described above for **3** gave 5.1 g (68%) of **4**. IR (Nujol): 1810 (vs), 1747 (vs), 1415 (m), 1294 (m), 1275 (m), 1080 (w, br), 945 (s), 930 (s, br), 915 (sh), 900 (s), 865 (m), 838 (m), 795 (w), 730 (s), 705 (s), 645 (s, br). ^{1}H NMR (250 MHz, DMSO-d_6) (δ): 1.38 (t, 24 H, PCH_3, J_{PH} = 6 Hz); 1.80 (d, 8 H, PCH_2, J_{PH} = 4 Hz). Mass spectrum (FAB$^+$, 2-nitrophenyl octyl ether): m/e 484 ([^{12}C$_{14}^1$H$_{32}^{35}$Cl^{16}O$_2^{31}$P$_4$-^{93}Nb]$^+$), 456 ([P − CO]$^+$), 428 ([P − 2CO]$^+$).

[Nb(CO)$_2$(dmpe)$_2$I] (5). This compound is formed as a side product (~5%) in the synthesis of **4** when the Mg(anthracene) catalytic system is used immediately (20 min) after the addition of MeI to activate the Mg. A crystal of **5** was picked out from the crystalline mixture of **4** and **5** that results from this synthesis and identified by X-ray crystallography (vide infra). A mass spectrum of the mixture also showed the presence of **5**. Mass spectrum (FAB$^+$, 2-nitrophenyl octyl ether): m/e 576 ([^{12}C$_{14}^1$H$_{32}^{127}$I^{16}O$_2^{31}$P$_4^{93}$Nb]$^+$), 548 ([P − CO]$^+$), 520 ([P − 2CO]$^+$), 484 ([^{12}C$_{14}^1$H$_{32}^{35}$Cl^{16}O$_2^{31}$P$_4^{93}$Nb]$^+$), 456 ([P − CO]$^+$), 428 ([P − 2CO]$^+$).

[Ta(CO)$_2$(depe)$_2$Cl] (6). To a stirred chilled (−30 °C) mixture of 50 mL of toluene and 10 mL of THF was added 1.0 g (4.85 mmol) of depe, followed by 0.868 g (2.42 mmol) of TaCl$_5$. A bright yellow precipitate formed immediately. The solution was stirred rapidly at room temperature with an amalgam comprised of 0.125 g of Na (5.43 mmol) and 16 g of Hg. After 6 h the green blue solution was allowed to settle, decanted from the solids, and evaporated to leave a gummy dark green solid, presumed to be [TaCl$_4$(depe)$_2$]. This material was dissolved in 20 mL of THF and a mixture of 0.080 g of Mg/0.080 g of HgCl$_2$/1–2 mg of anthracene (catalytic Mg/anthracene) was added. The solution was then stirred rapidly under 8–10 psig CO for 3 days, during which time the color turned dark brown. Compound **6** was isolated after chromatography of this solution through alumina and elution with THF, removal of the solvent, and washing with a small amount of pentane. Yield: 0.606 g (37%) of **6**. ^{1}H NMR (C_6D_6) (δ): 2.27 (4 H, m), 2.00 (4 H, m), 1.76 (8 H), 1.46 (4 H, m), 1.08 (16 H, m), 0.95 (12 H, m). ^{13}C{^{1}H} NMR (C_6D_6) (δ): 8.20 (s), 9.10 (s), 17.1 (quintet, J_{PC} = 23 Hz), 19.0 (quintet, J_{PC} = 22 Hz), 21.6 (quintet, J_{PC} = 33 Hz), 274.9 (quintet, J_{PC} = 44 Hz). ^{31}P{^{1}H} NMR (C_6D_6) (δ): 42.0 (s). FTIR (Nujol): 1819 (s), 1746 (s), 1029 (m), 981 (w), 875 (w), 760 (m), 736 (m), 711 (m), 662 (w) cm^{-1}. Anal. Calcd for $C_{22}H_{48}ClO_2P_4Ta$: C, 38.58; H, 7.06; N, 0.00; P, 18.09. Found: C, 38.75; H, 7.00; N, 0.00; P, 17.75.

[V(CO)$_2$(dmpe)$_2$Me] (8). Into a stirred solution of 0.144 g of Na[V(CO)$_2$(dmpe)$_2$] (0.335 mmol) in 20 mL of THF at −30 °C was syringed 38 μL (1 equiv) of MeOTf. The solution immediately turned red brown and was allowed to warm to room temperature. After 5 min the solvent was removed under vacuum and the product extracted into 20 mL of Et_2O. Evaporation yielded 0.127 g of a red orange mixture of [V(CO)$_2$-(dmpe)$_2$][36] and **8**, as determined by FTIR and ^{1}H and ^{31}P{^{1}H} NMR spectroscopy. Similar results were obtained by using DME instead of THF as solvent or by addition of MeOTf to Na[V(CO)$_2$(dmpe)$_2$] at −78 °C. Yellow compound **8** can be freed of [V(CO)$_2$(dmpe)$_2$] by successive recrystallization from Et_2O but with substantial loss of material (isolated yield 0.02 g, 14%). ^{1}H NMR (300 MHz, C_6D_6) (δ): 1.19 (s, 32 H, PCH_3), −1.80 (br quintet, J_{HP} = 12 Hz, VCH_3). ^{31}P{^{1}H} NMR (121 MHz, C_6D_6) (δ): 64 (br mult, unresolved). FTIR (Nujol): 1794 (s), 1731 (s), 1416 (w), 1282 (m), 1168 (w), 933 (s), 892 (w), 833 (w), 721 (m), 693 (m), 629 (m) cm^{-1}. Anal. Calcd for $C_{15}H_{35}O_2P_4V$: C, 42.66; H, 8.35; N, 0.00. Found: C, 42.78; H, 8.27; N, 0.00.

(34) Bogdanovic, B.; Liao, S.; Mynott, R.; Schlichte, K.; Westeppe, U. *Chem. Ber.* **1984**, *117*, 1378.
(35) Manzer, L. E. *Inorg. Chem.* **1977**, *16*, 525.
(36) Wells, F. J.; Wilkinson, G.; Motevalli, M.; Hursthouse, M. B. *Polyhedron* **1987**, *6*, 1351.

Table I. Crystallographic Information for $[TaCl_2(dmpe)_2]$ (**1**), $[Ta(\eta^4\text{-}C_{14}H_{10})(dmpe)_2Cl]\cdot 0.5C_6D_6$ (**2**·0.5C_6D_6), $[Nb(CO)_2(dmpe)_2Cl]$ (**4**), $[Nb(CO)_2(dmpe)_2I]$ (**5**), $[Ta(CO)_2(depe)_2Cl]$ (**6**), $[Ta(CO)_2(dmpe)_2Me]$ (**7**), and $[V(CO)_2(dmpe)_2Me]$ (**8**)[a]

	1	**2**·0.5C_6D_6	**4**	**5**	**6**	**7**	**8**
a, Å	9.384 (1)	12.997 (6)	16.106 (3)	16.571 (2)	11.245 (1)	10.615 (1)	13.509 (3)
b, Å	12.863 (2)	13.495 (3)	8.333 (1)	16.632 (2)	13.325 (2)	33.123 (7)	13.777 (2)
c, Å	9.363 (1)	18.860 (4)	33.881 (5)	8.439 (1)	10.881 (2)	12.766 (2)	11.719 (2)
α, deg		75.38 (2)			99.58 (1)		
β, deg	95.04 (1)	84.75 (5)			112.44 (1)		
γ, deg		89.50 (5)			70.24 (1)		
V, Å^3	1125.7 (4)	3187 (3)	4547 (2)	2325.9 (8)	1416.9 (4)	4488 (2)	2181.2 (7)
temp, °C	22	21	25	24	−80	23	−78
fw, g mol^{-1}	552.0	733.6	484.5	575.9	684.9	552.3	422.3
Z	2	4	8	4	2	8	4
ρ_{calc}, g cm^{-3}	1.63	1.53	1.42	1.65	1.61	1.64	1.29
space group	$P2_1/n$ (No. 14)	$P\bar{1}$ (No. 2)	$Pna2_1$ (No. 33)	*Pnma* (No. 62)	$P\bar{1}$ (No. 2)	*Fdd*2 (No. 43)	$P2_12_12_1$ (No. 19)
2θ limit, deg	$3 \le 2\theta \le 46$	$3 \le 2\theta \le 46$	$3 \le 2\theta \le 50$	$3 \le 2\theta \le 55$	$3 \le 2\theta \le 50$	$3 \le 2\theta \le 64$	$3 \le 2\theta \le 46$
data limits	$\pm h,+k,+l$	$\pm h,\pm k,+l$	$+h,+k,+l$	$+h,+k,+l$	$+h,\pm k,\pm l$	$+h,+k,+l$	$+h,+k,+l$
μ, cm^{-1}	51.7	36.0	9.06	19.8	41.7	51.3	7.3
tot. no. of data	1453	11118	4223	2753	6499	4647	2559
no. of unique data[b]	1130	7734	2828	1818	4693	1823	1736
no. of param	88	631	396	117	415	100	199
p	0.05	0.05	0.03	0.05	0.03	0.05	0.03
R[c]	0.030	0.043	0.045	0.038	0.018	0.029	0.050
R_w	0.039	0.063	0.060	0.046	0.023	0.037	0.055

[a] Data were collected on an Enraf Nonius CAD-4F κ-geometry diffractometer using Mo Kα radiation. [b] Observation criterion $I > 2\sigma(I)$, except for **4**, **6**, **7**, and **8**, where $I > 3\sigma(I)$. [c] $R = \sum||F_o| - |F_c||/\sum|F_o|$, $R_w = [\sum w(|F_o| - |F_c|)^2/\sum w|F_o|^2]^{1/2}$, where the function minimized is $[\sum w(|F_o| - |F_c|)^2]^{-1}$ and w is defined in ref 10.

Collection and Reduction of X-ray Data. Data collection and reduction for complexes **1**, **2**, and **4**–**8** were carried out as previously described,[37] details of which are presented in Table I.

$[TaCl_2(dmpe)_2]$ (1). A red crystal, grown by cooling a pentane solution of **1** to −20 °C, was used in the diffraction study. The crystal, a prism of dimensions 0.3 × 0.25 × 0.2 mm, was sealed in a capillary tube under an atmosphere of nitrogen. Study on the diffractometer showed $2/m$ Laue symmetry and systematic absences ($h0l$, $h + l = 2n + 1$; $0k0$, $k = 2n + 1$) consistent the space group $P2_1/n$ (C_{2h}^5, No. 14). The data were corrected for extensive crystal decay (50%) during data collection but not for absorption.

$[Ta(\eta^4\text{-anthracene})(dmpe)_2Cl]\cdot 0.5C_6D_6$ (2·0.5C_6D_6). An orange crystal grown by slow evaporation of a benzene-d_6 solution of **2** was used in the diffraction study. The crystal, a parallelepiped of approximate dimensions 0.5 × 0.12 × 0.25 mm and bounded by {100}, {010}, and {001}, was mounted in a capillary tube under nitrogen. Study on the diffractometer showed only triclinic symmetry ($\bar{1}$), consistent with the space group $P1$ (C_1^1, No. 1) or $P\bar{1}$ (C_i^1, No. 2). An empirical absorption correction was applied to the data.

$[Nb(CO)_2(dmpe)_2Cl]$ (4). An orange crystal grown by slow evaporation of a benzene solution of **4** was used in the diffraction study. The crystal, a parallelepiped of approximate dimensions 0.6 × 0.35 × 0.17 mm and bounded by {100}, {001}, and {01$\bar{1}$}, was sealed in a capillary tube under an atmosphere of nitrogen. Study on the diffractometer showed *mmm* Laue symmetry and systematic absences ($0kl$, $k + l = 2n + 1$; $h0l$, $h = 2n + 1$) consistent with the space groups $Pna2_1$ (C_{2v}^9, No. 33) or *Pnam* (nonstandard setting of *Pnma*, D_{2h}^{16}, No. 62). An empirical absorption correction was applied to the data.

$[Ta(CO)_2(dmpe)_2Cl]$ (3). The unit cell parameters of an orange crystal of **3** grown by slow evaporation of a benzene solution of **3** were identical to those of **4**, revealing the two compounds to be isomorphous and probably isostructural.

$[Nb(CO)_2(dmpe)_2I]$ (5). An orange crystal grown by slow evaporation of a benzene solution of **5** was used in the diffraction study. The crystal, a parallelepiped of approximate dimensions 0.42 × 0.18 × 0.38 mm and bounded by {100}, {010}, and {001}, was sealed in a capillary tube under an atmosphere of nitrogen. Study on the diffractometer showed *mmm* Laue symmetry and systematic absences ($0kl$, $k + l = 2n + 1$; $hk0$; $h = 2n + 1$) consistent with the space groups $Pn2_1a$ (nonstandard setting of $Pna2_1$, C_{2v}^9, No. 33) or *Pnma* (D_{2h}^{16}, No. 62). An empirical absorption correction was applied to the data.

$[Ta(CO)_2(depe)_2Cl]$ (6). Yellow crystals of **6** were grown from a solution of **6** cooled to −30 °C. A crystal of dimensions 0.20 × 0.22 × 0.20 mm was mounted at the end of a quartz fiber with silicon grease on a cold stage. The crystal was judged to be acceptable on the basis of open counter ω-scans of several low-angle reflections ($\Delta\tilde{\omega} = 0.21°$). Study on the diffractometer showed only triclinic symmetry ($\bar{1}$), consistent with the space group $P1$ (C_1^1, No. 1) or $P\bar{1}$ (C_i^1, No. 2). An empirical absorption correction was applied to the data.

$[Ta(CO)_2(dmpe)_2Me]$ (7). An orange crystal of **7** was used in the diffraction study. The crystal, a block of approximate dimensions 0.28 × 0.35 × 0.46 mm, was sealed in a capillary tube under an atmosphere of nitrogen. Study on the diffractometer revealed *mmm* Laue symmetry and systematic absences consistent with the space group *Fdd*2 (C_{2v}^{19}, No. 43).

$[V(CO)_2(dmpe)_2Me]$ (8). Multifaceted yellow crystals of **8** were grown from a solution of **8** cooled to −30 °C. A crystal of dimensions 0.20 × 0.20 × 0.30 mm was mounted on the end of quartz fiber with silicon grease on a cold stage. Study on the diffractometer revealed $2/m$ Laue symmetry and systematic absences ($h0l$, $l = 2n + 1$) consistent with the space group $P2_12_12_1$ (D_2^4, No. 19).

Determination and Refinement of the Structures. The tantalum atom in $[TaCl_2(dmpe)_2]$ (**1**) was placed on a special position at the origin of the cell. Phasing from this solution revealed the location of the remaining non-hydrogen atoms by successive difference Fourier maps. All non-hydrogen atoms were refined with anisotropic thermal parameters. Hydrogen atoms were placed in calculated positions (d_{C-H} = 0.95 Å), constrained to "ride" on the carbons to which they were attached, and given a fixed common isotropic thermal parameter. Calculations were performed by using SHELX-76,[38] with neutral-atom scattering factors and anomalous dispersion corrections for the non-hydrogen atoms.[39] Refinement converged to the R-factors reported in Table I. The final difference Fourier map showed a peak of 1.4 e Å^{-3} located near the Ta atom. Final non-hydrogen positional parameters are given in Table S1 (supplementary material), final non-hydrogen thermal parameters are given in Table S2, and final hydrogen positional and thermal parameters are given in Table S3.

$[Ta(\eta^4\text{-anthracene})(dmpe)_2Cl]\cdot 0.5C_6D_6$ (2·0.5C_6D_6) was solved in the space group $P\bar{1}$ following a Patterson synthesis, which revealed the positions of two independent Ta atoms in the asymmetric unit. The other non-hydrogen atoms were subsequently located in successive difference Fourier maps, which revealed the presence of a benzene solvate molecule. All non-hydrogen atoms were refined with anisotropic thermal parameters. Hydrogen atom positions were calculated, constrained to "ride" on the carbon atoms to which they were attached, and given a fixed common isotropic thermal parameter as in **1**. Least-squares refinement converged at the R-factors reported in Table I. The final difference Fourier map showed a peak of 1.5 e Å^{-3} located near a Ta atom. Final non-hydrogen atom positional parameters are reported in Table S5, final non-hydrogen

(37) Silverman, L. D.; Dewan, J. C.; Giandomenico, C. M.; Lippard, S. J. *Inorg. Chem.* **1980**, *19*, 3379.

(38) Sheldrick, G. M. SHELX-76, a package of crystallographic programs.

(39) *International Tables For X-ray Crystallography*; Kynoch Press: Birmingham, England, 1974.

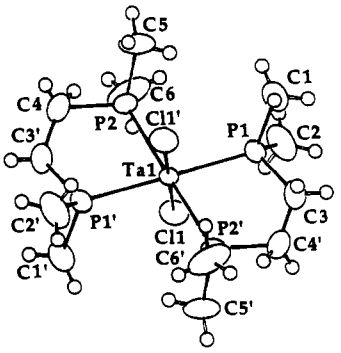

Figure 1. ORTEP view of $[TaCl_2(dmpe)_2]$ (**1**), showing 40% thermal ellipsoids.

thermal parameters are reported in Table S6, and final hydrogen positional and thermal parameters are reported in Table S7.

The structure of $[Nb(CO)_2(dmpe)_2Cl]$ (**4**) was solved in the noncentrosymmetric space group $Pna2_1$, by standard Patterson and difference Fourier techniques, requiring two crystallograpically independent molecules per asymmetric unit. Calculations were performed using TEXSAN.[40] All non-hydrogen atoms were refined with anisotropic thermal parameters. Hydrogen atoms were placed at calculated positions during the final refinement cycles with isotropic thermal temperatures 1.2 times that of the connected carbon atoms. Refinement converged at the *R*-factors reported in Table I; refinement of the alternate hand of the structure resulted in a slight preference for the enantiomorph presented. The final difference Fourier map showed a peak of 1.2 e Å^{-3} located near Cl2. Final atom thermal parameters and *B*(eq) values are given in Table S9, and final anisotropic thermal parameters are given in Table S10.

The structure of $[Nb(CO)_2(dmpe)_2I]$ (**5**) was solved and refined by methods analogous to those reported above for **2**. The iodine and niobium atoms were located from a Patterson map and found to lie on the mirror plane. The mirror plane bisects each dmpe ligand, with the methylene carbons showing large anisotropic thermal parameters, reflecting disorder of these atoms across the mirror. The C–C bonds of the dmpe ligands are thus shortened due to librational effects. Hydrogen atom positions were treated as in **2**, with one common isotropic thermal parameter refined for the methyl hydrogens, and a separate one was refined for the hydrogens of the methylene groups. Least-squares refinement converged to the *R*-factors reported in Table I. The final difference Fourier map showed a residual peak of 1.08 e Å^{-3} located near Nb. Final non-hydrogen positional parameters are given in Table S12, final non-hydrogen thermal parameters are given in Table S13, and final hydrogen positional and thermal parameters are given in Table S14.

The tantalum atom in $[Ta(CO)_2(depe)_2Cl]$ (**6**) was located by direct methods. Remaining non-hydrogen atoms were revealed by subsequent least-squares refinements and difference Fourier maps. Calculations were performed using TEXSAN.[40] All non-hydrogen atoms were refined anisotropically. Hydrogen atoms were located and positions refined with isotropic thermal temperatures 1.2 times that of the connected carbon atoms. The largest residual peak in the final difference Fourier map was 0.34 e Å^{-3} located near C25. Final atom positional and *B*(eq) parameters are given in Table S16, and final anisotropic thermal parameters are given in Table S17.

$[Ta(CO)_2(dmpe)_2Me]$ (**7**) was solved and refined by methods analogous to those reported above for **6**. Patterson and difference Fourier maps revealed $^1/_2$ molecule of **7** per asymmetric unit, with a crystallographic 2-fold axis passing through the Ta atom and the methyl group and bisecting the two dmpe ligands. All non-hydrogen atoms were refined anisotropically. Hydrogen atoms were placed at calculated positions during the final refinement cycles with isotropic thermal temperatures 1.2 times that of the connected carbon atoms. Refinement of the alternate hand of the structure resulted in a substantial increase in R_2, from 0.037 to 0.063, confirming that the correct enantiomorph was originally chosen. The final difference Fourier map showed a residual peak of 1.63 e Å^{-3} located near Ta1 (no absorption correction was applied). Final atom positional and *B*(eq) parameters are given in Table S19, and final anisotropic thermal parameters are given in Table S20.

(40) TEXSAN: *Single Crystal Structure Analysis Software*; Molecular Structure Corp.: The Woodlands, Tx, 1989; Vol. 5.0.

Table II. Bond Lengths (Å) and Angles (deg) for $[TaCl_2(dmpe)_2]$ (**1**)[a]

Bond Lengths			
Ta1–Cl1	2.427 (2)	Ta1–P1	2.516 (2)
Ta1–P2	2.521 (2)	P1–C2	1.80 (1)
P1–C1	1.817 (9)	P1–C3	1.83 (1)
P2–C5	1.80 (1)	P2–C6	1.827 (9)
P2–C4	1.86 (1)	C3–C4	1.48 (1)
Bond Angles			
Cl1–Ta1–Cl1′	180.0	Cl1–Ta1–P1	90.69 (6)
Cl1–Ta1–P1′	89.31 (6)	Cl1–Ta1–P2′	91.28 (6)
Cl1–Ta1–P2	88.72 (6)	P1–Ta1–P1′	180.0
P1–Ta1–P2′	77.40 (6)	P1–Ta1–P2	102.60 (6)
P2–Ta1–P2′	180.0	C2–P1–C1	100.2 (5)
C2–P1–C3	106.5 (5)	C2–P1–Ta1	118.4 (4)
C1–P1–C3	98.0 (4)	C1–P1–Ta1	119.9 (3)
C3–P1–Ta1	111.2 (3)	C5–P2–C6	100.7 (5)
C5–P2–C4	100.4 (5)	C5–P2–Ta1	121.0 (4)
C6–P2–C4	103.6 (5)	C6–P2–Ta1	117.7 (3)
C4–P2–Ta1	110.8 (3)	C4–C3–P1	112.6 (8)
C3–C4–P2	110.8 (7)		

[a] See Figure 1 for atom-labeling scheme. Numbers in parentheses are estimated standard deviations in the last digit(s) given.

The vanadium atom in $[V(CO)_2(dmpe)_2Me]$ (**8**) was located by direct methods. Remaining non-hydrogen atoms were revealed by subsequent least-squares refinements and difference Fourier maps. All non-hydrogen atoms were refined anisotropically. Hydrogen atom positions were calculated as in **7**. The largest residual peak in the final difference Fourier map was 0.58 e Å^{-3} located near C3. Final atom positional and *B*(eq) parameters are given in Table S22, and final anisotropic thermal parameters are given in Table S23.

Results and Discussion

When 1 equiv of Mg(anthracene)·3THF is added to a THF solution of the Ta(IV) complex $[TaCl_4(dmpe)_2]$, it is rapidly reduced to the known compound $[TaCl_2(dmpe)_2]$ (**1**) (eq 1),[27,33]

$$[TaCl_4(dmpe)_2] + Mg(C_{14}H_{10})\cdot 3THF \xrightarrow{THF} \underset{\mathbf{1}}{[TaCl_2(dmpe)_2]} \quad (1)$$

which was identified by crystallography and by its EPR spectrum. Although this reaction appears to be extremely efficient, it offers no advantage over the literature method involving reduction of $[TaCl_4(dmpe)_2]$ with Na/Hg, for anthracene cannot be easily separated from **1**. We were successful, however, in growing X-ray-quality crystals of **1**, the molecular structure of which is shown in Figure 1. Details of the molecular geometry are summarized in Table II. As deduced from its solubility, and by analogy to the structure of $[Ta(PMe_3)_4Cl_2]$, **1** exhibits a trans octahedral geometry. The Ta–Cl bond length of 2.427 (2) Å is slightly shorter than the reported value of 2.464 (3) Å for the Ta–Cl bonds in $[Ta(PMe_3)_4Cl_2]$ as are the two Ta–P bond distances, 2.516 (2) and 2.521 (2) Å, compared with the Ta–P bond length of 2.543 (2) Å in $[Ta(PMe_3)_4Cl_2]$. These differences reflect the greater steric demands of four trimethylphosphine versus two dmpe ligands.

As shown in eq 2, reaction of $[TaCl_4(dmpe)_2]$ with excess $Mg(C_{14}H_{10})\cdot 3THF$ (1:1.5) in THF led to rapid formation of orange-red $[Ta(\eta^4\text{-}C_{14}H_{10})(dmpe)_2Cl]$ (**2**), which was purified

$$\underset{\mathbf{1}}{[TaCl_4(dmpe)_2]} + 1.5Mg(C_{14}H_{10})\cdot 3THF \xrightarrow{THF} \underset{\mathbf{2}}{[Ta(\eta^4\text{-}C_{14}H_{10})(dmpe)_2Cl]} \quad (2)$$

by column chromatography on alumina. The molecular structure of the two crystallographically independent molecules (A and B) in the crystals of $\mathbf{2}\cdot 0.5C_6D_6$ are shown in Figure 2. Table III

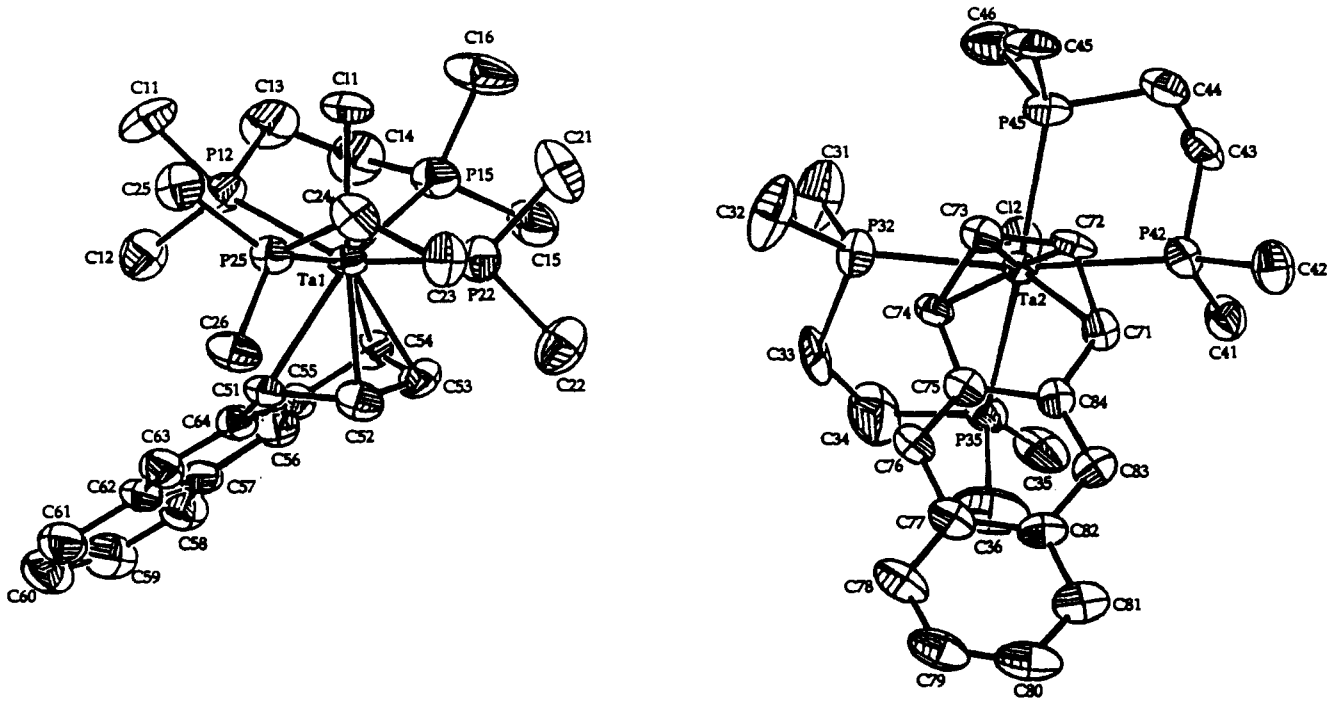

Figure 2. ORTEP view of $[Ta(\eta^4\text{-}C_{14}H_{10})(dmpe)_2Cl]\cdot 0.5C_6D_6$ ($2\cdot 0.5C_6D_6$), molecule A (left) and B (right), showing 40% thermal ellipsoids.

summarizes the molecular geometry. Transition metal η^2-, η^3-, η^4-, and η^6-anthracene complexes have been structurally characterized.[41-45] The closely related complex $[Ta(\eta^4\text{-}C_{10}H_8)(dmpe)_2Cl]$ has been prepared by addition of 3 equiv of sodium naphthalenide to a solution of $[TaCl_4(dmpe)_2]$.[46] The molecular geometry of **2**, like that of $[Ta(\eta^4\text{-}C_{10}H_8)(dmpe)_2Cl]$, may be considered as approximately pentagonal bipyramidal, with the midpoints (for molecule A) of the C51–C52 and C53–C54 bonds, Ta1, P15, P25, and Cl1 forming the pentagonal plane and P12 and P22 the apices of the bipyramid (Figure 2). All deviations from the plane are less than 0.12 Å. The P22–Ta1–P12 angle of 154.87 (9)° is distorted from idealized pentagonal bipyramidal geometry, presumably due to the chelating nature of the dmpe ligands. Molecule B adopts a similar geometry, with the midpoints of the C71–C72 and C73–C74 bonds, Ta2, P32, P42, and Cl2 forming the pentagonal plane and P35 and P45 the apices of the bipyramid (Figure 2). The dihedral angles between the η^4-diene fragment and the remaining uncoordinated anthracene fragments are 42.2 and 42.9° for molecules A and B. Other structurally characterized η^4-arene complexes exhibit similar dihedral angles.[44,46-52] The C52–Ta1 and C53–Ta1 (C72–Ta2 and C73–Ta2) bond lengths are more than 0.1 Å shorter than the C51–Ta1 and C54–Ta1 (C71–Ta2 and C74–Ta2) distances; the C52–C53 (C72–C73) distances are also shorter than the C51–C52 and C53–C54 (C71–C72 and C73–C74) bond distances, although these are much closer to being identical. Similar variations were also observed in the molecular geometry of $[Ta(\eta^4\text{-}C_{10}H_8)(dmpe)_2Cl]$.[46] The C–C distances in the uncoordinated anthracene fragment in **2** compare favorably to those found in $[Ta(\eta^4\text{-}C_{10}H_8)(dmpe)_2Cl]$ and $[Co(\eta^4\text{-}C_{14}H_{10})(SnPh_3)(PMe_3)_2]$,[44] where the arenes are tightly bound due to substantial π-donation from the metal to the complexed diene. These three complexes do not react with CO to displace the arene moiety.

The anthracene ligand in **2** also cannot be substituted or removed by alkynes or isocyanides, and **2** forms preferentially even in the presence of these ligands when excess $Mg(C_{14}H_{10})\cdot 3THF$ reacts with $[TaCl_4(dmpe)_2]$.[53] The stability and preferred formation of complexes such as **2** and $[Ta(\eta^4\text{-}C_{10}H_8)(dmpe)_2Cl]$ are the probable reasons for the low yield of $[Ta(CO)_2(dmpe)_2Cl]$ when synthesized by reduction of $[TaCl_4(dmpe)_2]$ with sodium naphthalenide in the presence of CO.[33] Complex **2** does not appear to be reduced further by reaction with excess $Mg(C_{14}H_{10})\cdot 3THF$; however, when $[TaCl_4(dmpe)_2]$ is reduced by activated Mg metal in THF, a Ta(I) complex (^{31}P NMR, δ = 20–22 ppm) is apparently produced.[53] This compound may be $[Ta(dmpe)_2Cl]_2(\mu\text{-}N_2)$, by analogy with reported Nb and Ta chemistry using PMe_3 in place of dmpe.[23,24]

The ^1H, $^{13}C\{^1H\}$, and $^{31}P\{^1H\}$ NMR spectra of **2** at room temperature closely parallel those of $[Ta(\eta^4\text{-}C_{10}H_8)(dmpe)_2Cl]$ at higher temperatures (55 °C). The $^{31}P\{^1H\}$ NMR spectrum of **2** at room temperature is a singlet (δ = 12.6 ppm). The ^1H spectrum exhibits a singlet for H73 and H83 at δ = 6.42 ppm, two complex multiplets (δ = 6.9, 7.1) for H78–H79 and H80–H81, and broad resonances for the dmpe methyl and methylene groups centered at δ = 1.41 and 1.82 ppm. The ^1H resonances attributed to H71–H74 are presumably obscured by the dmpe peaks, as was the case for $[Ta(\eta^4\text{-}C_{10}H_8)(dmpe)_2Cl]$. These spectral features are consistent with an equivalent environment for the four phosphorus atoms and the presence of an effective mirror plane through the anthracene ligand. The $^{13}C\{^1H\}$ NMR spectrum of **2** confirms both these observations; distinct resonances appear in the aromatic region for all carbons (C76–C84) of half the anthracene moiety, while a broad upfield resonance at δ = 61.0 ppm arises from the coordinated η^4-diene carbons. Two

(41) Brauer, D. J.; Krüger, C. *Inorg. Chem.* **1977**, *16*, 884.
(42) Griffith, E. A. H.; Amma, E. L. *J. Am. Chem. Soc.* **1974**, *96*, 5407.
(43) Begley, M. J.; Puntambekar, S. G.; Wright, A. H. *J. Chem. Soc., Chem. Commun.* **1987**, 1251.
(44) Klein, H.-F.; Ellrich, K.; Lamac, S.; Lull, G.; Zsolnai, L.; Huttner, G. *Z. Naturforsch.* **1985**, *40b*, 1377.
(45) Hanic, F.; Mills, O. S. *J. Organomet. Chem.* **1968**, *11*, 151.
(46) Albright, J. O.; Datta, S.; Dezube, B.; Kouba, J. K.; Marynick, D. S.; Wreford, S. S.; Foxman, B. M. *J. Am. Chem. Soc.* **1979**, *101*, 611.
(47) Churchill, M. R.; Mason, R. *Proc. R. Soc. London, Ser. A* **1966**, *292*, 61.
(48) Herbstein, F. H.; Reisner, M. G. *J. Chem. Soc., Chem. Commun.* **1972**, 1077.
(49) Huttner, G.; Lange, S.; Fischer, E. O. *Angew. Chem., Int. Ed. Engl.* **1971**, *10*, 556.
(50) Huttner, G.; Lange, S. *Acta Crystallogr., Sect. B* **1972**, *28*, 2049.
(51) Barlex, D. M.; Evans, J. A.; Kemmitt, R. D. W.; Russell, D. R. *J. Chem. Soc., Chem. Commun.* **1971**, 331.
(52) Bond, A.; Bottrill, M.; Green, M.; Welch, A. J. *J. Chem. Soc., Dalton Trans.* **1977**, 2372.
(53) Bianconi, P. A.; Lippard, S. J. Unpublished results.

Table III. Selected Bond Lengths (Å) and Angles (deg) for $[Ta(\eta^4\text{-}C_{14}H_{10})(dmpe)_2Cl]\cdot 0.5C_6H_6$ (**2**)[a]

molecule A		molecule B	
	Bond Lengths		
Ta1–Cl1	2.582 (3)	Ta2–Cl2	2.583 (3)
Ta1–P12	2.584 (4)	Ta2–P32	2.622 (2)
Ta1–P15	2.622 (3)	Ta2–P35	2.589 (3)
Ta1–P22	2.567 (3)	Ta2–P42	2.632 (2)
Ta1–P25	2.625 (3)	Ta2–P45	2.579 (3)
Ta1–C51	2.419 (9)	Ta2–C71	2.379 (9)
Ta1–C52	2.27 (1)	Ta2–C72	2.245 (9)
Ta1–C53	2.26 (1)	Ta2–C73	2.28 (1)
Ta1–C54	2.38 (1)	Ta2–C74	2.39 (1)
	Bond Angles		
C51–Ta1–Cl1	143.2 (3)	C71–Ta2–Cl2	143.3 (2)
C52–Ta1–Cl1	150.6 (3)	C72–Ta2–Cl2	150.1 (3)
C53–Ta1–Cl1	151.9 (2)	C73–Ta2–Cl2	152.3 (2)
C54–Ta1–Cl1	145.4 (3)	C74–Ta2–Cl2	145.3 (2)
P12–Ta1–Cl1	77.5 (1)	P32–Ta2–Cl2	74.96 (8)
P15–Ta1–Cl1	76.0 (1)	P35–Ta2–Cl2	77.76 (9)
P22–Ta1–Cl1	77.8 (1)	P42–Ta2–Cl2	71.71 (8)
P25–Ta1–Cl1	70.71 (9)	P45–Ta2–Cl2	77.90 (9)
P12–Ta1–P15	77.1 (1)	P32–Ta2–P35	77.46 (8)
P12–Ta1–P22	154.87 (9)	P32–Ta2–P42	146.52 (8)
P12–Ta1–P25	99.34 (9)	P32–Ta2–P45	94.1 (1)
P15–Ta1–P22	92.8 (1)	P35–Ta2–P42	98.24 (8)
P15–Ta1–P25	146.45 (9)	P35–Ta2–P45	155.55 (8)
P22–Ta1–P25	76.29 (9)	P42–Ta2–P45	76.1 (1)
C51–Ta1–P12	89.8 (2)	C71–Ta2–P32	136.6 (3)
C51–Ta1–P15	135.0 (2)	C71–Ta2–P35	90.5 (2)
C51–Ta1–P22	112.8 (2)	C71–Ta2–P42	75.9 (3)
C51–Ta1–P25	77.7 (2)	C71–Ta2–P45	110.6 (2)
C52–Ta1–P12	124.0 (3)	C72–Ta2–P32	125.1 (3)
C52–Ta1–P15	125.1 (3)	C72–Ta2–P35	125.0 (2)
C52–Ta1–P22	80.7 (3)	C72–Ta2–P42	84.9 (3)
C52–Ta1–P25	84.9 (3)	C72–Ta2–P45	78.7 (2)
C53–Ta1–P12	121.8 (2)	C73–Ta2–P32	88.4 (2)
C53–Ta1–P15	88.1 (3)	C73–Ta2–P35	120.7 (2)
C53–Ta1–P22	80.1 (2)	C73–Ta2–P42	120.7 (3)
C53–Ta1–P25	120.2 (3)	C73–Ta2–P45	81.4 (2)
C54–Ta1–P12	86.2 (2)	C74–Ta2–P32	71.9 (2)
C54–Ta1–P15	70.7 (2)	C74–Ta2–P35	85.4 (2)
C54–Ta1–P22	112.4 (2)	C74–Ta2–P42	141.4 (2)
C54–Ta1–P25	142.8 (2)	C74–Ta2–P45	114.1 (2)
C51–Ta1–C52	36.2 (4)	C71–Ta2–C72	36.8 (3)
C51–Ta1–C53	62.6 (3)	C71–Ta2–C73	62.1 (3)
C51–Ta1–C54	65.5 (3)	C71–Ta2–C74	65.6 (3)
C52–Ta1–C53	37.0 (4)	C72–Ta2–C73	36.7 (4)
C52–Ta1–C54	62.4 (4)	C72–Ta2–C74	62.7 (4)
C53–Ta1–C54	36.5 (3)	C73–Ta2–C74	36.2 (3)

bond types	min	max	mean[b]
P-C	1.79 (2)	1.86 (1)	1.83
CH_2-CH_2	1.41 (2)	1.52 (2)	1.49
C-C(aromatic)	1.35 (1)	1.48 (1)	1.42

[a] See Figure 2 for atom-labeling scheme. Numbers in parentheses are estimated standard deviations in the last digit(s) given. [b] The mean values are the average for the individual values including molecules A and B.

peaks are seen for the dmpe methyl groups (at δ = 17.8 and 14.6 ppm) and one for the methylene carbons, similar to those occurring in seven-coordinate capped trigonal prismatic complexes containing the dmpe ligand. The dmpe methyl groups directed toward the capping ligand are resolved from those directed at the anthracene moiety, as was seen for $[Ta(\eta^4\text{-}C_{10}H_8)(dmpe)_2Cl]$. The equivalence of four methyl carbons in these two environments reflects the equivalence of the four phosphorus sites.

The identical characteristics of the spectra of **2** and of $[Ta(\eta^4\text{-}C_{10}H_8)(dmpe)_2Cl]$ reveal that similar fluxional processes are occurring in both. Extensive analysis of the fluxionality of $[Ta(\eta^4\text{-}C_{10}H_8)(dmpe)_2Cl]$ by variable-temperature NMR studies led to the conclusion that the bound naphthalene moiety rotates about the Ta–Cl vector, thus averaging the phosphorus environments and creating the effective mirror plane through the naphthalene ligand.[46] For **2**, the observation of distinct ^1H and ^{13}C resonances

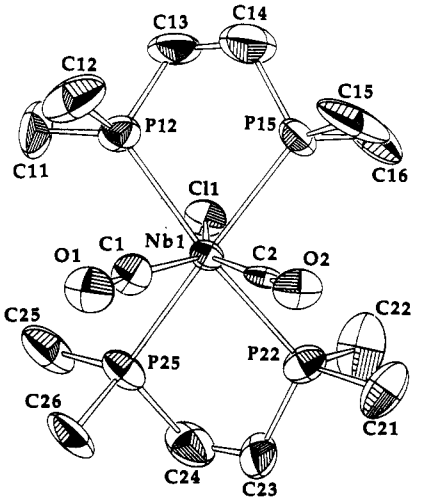

Figure 3. ORTEP view of $[Nb(CO)_2(dmpe)_2Cl]$ (**4**), showing 40% thermal ellipsoids.

for the coordinated and free portions of the anthracene rules out processes involving complete dissociation of the ligand or migration of Ta between aromatic rings. Some fluxionality must occur to account for the averaging of the phosphorus and dmpe methyl carbon environments and the mirror symmetry of the anthracene fragment, however. Rotation of the bound anthracene moiety around the Ta–Cl vector of **2**, analogous to that found for $[Ta(\eta^4\text{-}C_{10}H_8)(dmpe)_2Cl]$, is the most likely possibility. This type of fluxionality contrasts to that recently reported for $[Ni(\eta^4\text{-}C_{14}H_{10})(PR_3)_2]$ (R = Et, Bu), where the $Ni(PR_3)_2$ fragment is observed to migrate between the two ends of the coordinated anthracene.[54]

Although reduction of $[TaCl_4(dmpe)_2]$ with $Mg(C_{14}H_{10})\cdot 3THF$ in the presence of CO does not yield $[Ta(CO)_2(dmpe)_2Cl]$, replacement of $Mg(C_{14}H_{10})\cdot 3THF$ with the catalytic $Mg(C_{14}H_{10})$ system affords very good yields of $[Ta(CO)_2(dmpe)_2Cl]$ (94%). Presumably, the low concentrations of anthracene present in solution are insufficient to drive the formation of $[Ta(\eta^4\text{-}C_{14}H_{10})(dmpe)_2Cl]$ (**2**). The same conditions also afford good yields of the niobium analogue $[Nb(CO)_2(dmpe)_2Cl]$ (**4**) (68%) from $[NbCl_4(dmpe)_2]$. $[Ta(CO)_2(dmpe)_2Cl]$ (**3**) was prepared previously by reduction of $[TaCl_4(dmpe)_2]$ with $Na(C_{10}H_8)$ under CO in only 46% yield,[33] possibly due to competitive formation of $[Ta(\eta^4\text{-}C_{10}H_8)(dmpe)_2Cl]$.

From the synthesis of $[Nb(CO)_2(dmpe)_2Cl]$ (**4**), X-ray-quality crystals of **4** and $[Nb(CO)_2(dmpe)_2I]$ (**5**) were obtained, the structures of which were determined. In the procedure involving catalytic $Mg(C_{14}H_{10})$, compound **5** can be isolated in low yields (~5%) if the prepared $Mg(C_{14}H_{10})$ system is used immediately (20 min) following addition of MeI to activate the Mg. As shown in Figures 3 and 4, complexes **4** and **5** both adopt capped trigonal prismatic geometries, with the halide ion in the capping position. Tables IV and V list important bond distances and angles for **4** and **5**, respectively. The Nb–Cl bond lengths in **4** are 2.702 (4) and 2.745 (3) Å, and the Nb–I bond distance in **5** is 2.9864 (8) Å. Other crystallographically determined Nb(I)–Cl and Ta(I)–Cl bond lengths range from 2.582 (3) to 2.6362 (7) Å.[46,55] The anomalously long Nb–Cl bonds of **4** may be due to a small amount of **5**, the iodide-capped analog of **4**, doped into the crystal lattice, because the crystal of **4** used in diffraction study was grown from a mixture of **4** and **5**.[31,56] These Nb–Cl and Nb–I distances are considerably longer than the Mo–Cl [2.537 (1) Å] and W–I [2.859 (3), 2.907 (3) Å] bond lengths in $[Mo(CO)_2(dmpe)_2Cl]PF_6$[57]

(54) Stanger, A.; Vollhardt, K. P. C. *Organometallics* **1992**, *11*, 317.
(55) Carnahan, E. M.; Rardin, R. L.; Bott, S. G.; Lippard, S. J. *Inorg. Chem.*, in press.
(56) Yoon, K.; Parkin, G. *J. Am. Chem. Soc.* **1991**, *113*, 8414.
(57) Fong, L. K.; Fox, J. R.; Foxman, B. M.; Cooper, N. J. *Inorg. Chem.* **1986**, *25*, 1880.

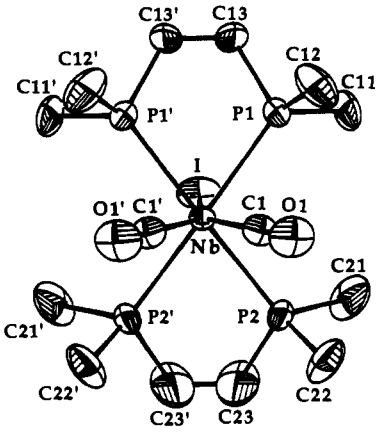

Figure 4. ORTEP view of $[Nb(CO)_2(dmpe)_2I]$ (**5**), showing 40% thermal ellipsoids.

Table IV. Selected Bond Lengths (Å) and Angles (deg) for $[Nb(CO)_2(dmpe)_2Cl]$ (**4**)[a]

molecule A		molecule B	
	Bond Lengths		
Nb1–Cl1	2.702 (3)	Nb2–Cl2	2.745 (3)
Nb1–P12	2.596 (5)	Nb2–P32	2.601 (5)
Nb1–P15	2.588 (5)	Nb2–P35	2.601 (5)
Nb1–P22	2.612 (5)	Nb2–P42	2.602 (5)
Nb1–P25	2.598 (5)	Nb2–P45	2.599 (5)
Nb1–C1	2.00 (2)	Nb2–C3	1.99 (2)
Nb1–C2	2.06 (2)	Nb2–C4	2.05 (2)
O1–C1	1.18 (2)	O3–C3	1.19 (2)
O2–C2	1.13 (2)	O4–C4	1.16 (2)
	Bond Angles		
C1–Nb1–C2	69.1 (6)	C3–Nb2–C4	69.4 (5)
C1–Nb1–P12	74.9 (5)	C3–Nb2–P35	75.2 (5)
C1–Nb1–P25	77.1 (5)	C3–Nb2–P42	76.8 (5)
C1–Nb1–P15	117.9 (5)	C3–Nb2–P45	118.0 (5)
C1–Nb1–P22	119.5 (5)	C3–Nb2–P32	114.8 (5)
C1–Nb1–Cl1	139.0 (5)	C3–Nb2–Cl2	144.3 (5)
C2–Nb1–P12	114.2 (4)	C4–Nb2–P35	116.7 (4)
C2–Nb1–P25	115.1 (4)	C4–Nb2–P42	116.6 (4)
C2–Nb1–P15	77.8 (4)	C4–Nb2–P45	77.2 (4)
C2–Nb1–Cl1	151.8 (4)	C4–Nb2–Cl2	146.2 (4)
P12–Nb1–P25	107.7 (2)	P35–Nb2–P42	103.4 (2)
P12–Nb1–P15	73.2 (1)	P35–Nb2–P45	164.5 (2)
P12–Nb1–P22	164.9 (2)	P35–Nb2–P32	73.1 (1)
P12–Nb1–Cl1	79.7 (2)	P35–Nb2–Cl2	81.2 (2)
P25–Nb1–P15	163.9 (2)	P42–Nb2–P45	73.7 (2)
P25–Nb1–P22	73.8 (2)	P42–Nb2–P32	165.7 (1)
P25–Nb1–Cl1	80.7 (1)	P42–Nb2–Cl2	83.2 (1)
P15–Nb1–P22	101.2 (2)	P45–Nb2–P32	105.7 (2)
P15–Nb1–Cl1	83.7 (2)	P45–Nb2–Cl2	83.3 (1)
P22–Nb1–Cl1	85.8 (2)	P35–Nb2–Cl2	81.2 (2)
O1–C1–Nb1	176 (2)	O3–C3–Nb2	175 (2)
O2–C2–Nb1	178 (1)	O4–C4–Nb2	179 (1)

bond types	min	max	mean[b]
P-CH_3	1.78 (2)	1.91 (2)	1.83
P-CH_2	1.69 (3)	1.94 (3)	1.83
CH_2-CH_2	1.28 (3)	1.38 (3)	1.34

[a] See Figure 3 for atom-labeling scheme. Numbers in parentheses are estimated standard deviations in the last digit(s) given. [b] The mean values are the average for the individual values including molecules A and B.

and $[W(CO)_2(dmpe)_2I]I$,[58] reflecting the larger size of Nb(I) compared with Mo(II) and W(II). Similarly, the two average Nb–P bond lengths of 2.600 Å are ~0.05 Å longer than their counterparts in the Mo and W structures. The Nb–P distances for both complexes compare well to those determined for $[Nb(CO)_2(dmpe)_2\{OAr\text{-}3,5\text{-}Me_2\}]$ (average Nb–P = 2.598 Å).[59] Similarly, the average Nb–CO distances of 2.025 and 1.990 Å

(58) Drew, M. G. B.; Wolters, A. P. *Acta Crystallogr., Sect. B* **1977**, *33*, 1027.

Table V. Selected Bond Lengths (Å) and Angles (deg) for $[Nb(CO)_2(dmpe)_2I]$ (**5**)[a]

	Bond Lengths		
Nb–I	2.9864 (8)	Nb–P1	2.604 (2)
Nb–P2	2.595 (2)	Nb–C1	1.990 (6)
P1–C11	1.794 (7)	P1–C12	1.789 (8)
P1–C13	1.797 (8)	P2–C21	1.802 (9)
P2–C22	1.788 (7)	P2–C23	1.799 (9)
O1–C1	1.185 (8)	C13–C13′	1.43 (2)
C23–C23′	1.36 (2)		
	Bond Angles		
C1–Nb–C1′	68.0 (4)	C1–Nb–P2	76.8 (2)
C1–Nb–P2′	115.9 (2)	C1–Nb–P1	76.5 (2)
C1–Nb–P1′	115.6 (2)	C1–Nb–I	146.0 (2)
P2–Nb–P2′	73.17 (7)	P2–Nb–P1	105.06 (5)
P2–Nb–P1′	165.93 (5)	P2–Nb–I	83.43 (4)
P1–Nb–P1′	73.12 (7)	P1–Nb–I	82.50 (4)
C12–P1–C11	99.1 (4)	C12–P1–C13	99.7 (4)
C12–P1–Nb	120.0 (3)	C11–P1–C13	101.4 (4)
C11–P1–Nb	119.5 (3)	C13–P1–Nb	113.6 (3)
C22–P2–C23	99.3 (5)	C22–P2–C21	100.0 (4)
C22–P2–Nb	120.0 (3)	C23–P2–C21	101.4 (4)
C23–P2–Nb	113.3 (3)	C21–P2–Nb	119.6 (3)
O1–C1–Nb	178.9 (5)	C13′–C13–P1	117.8 (3)
C23′–C23–P2	118.8 (3)		

[a] See Figure 4 for atom-labeling scheme. Numbers in parentheses are estimated deviations in the last digit(s) given. Standard deviations quoted for the average deviations for the individual values.

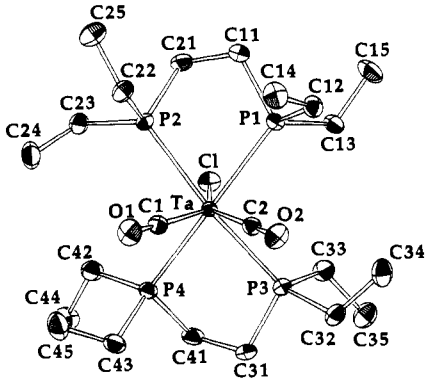

Figure 5. ORTEP view of $[Ta(CO)_2(depe)_2Cl]$ (**6**), showing 50% thermal ellipsoids.

for **4** and **5** match those for $[Nb(CO)_2(dmpe)_2\{OC_6H_5\text{-}3,5\text{-}Me_2\}]$ (average Nb–CO = 2.024 Å) and are shorter than the same distances in $[Nb(CO)_2(dppe)_2Cl]$ (average Nb–CO = 2.260 Å).[60]

The related complex $[Ta(CO)_2(depe)_2Cl]$ (**6**) was prepared in 37% yield in a manner similar to that employed for complex **3** and structurally characterized. As Figure 5 reveals, **6** also adopts a capped trigonal prismatic structure, bond distances and angles for which are listed in Table VI. Interestingly, the added steric bulk of the depe ligands compared to that in the dmpe analogues does not significantly reduce the OC–M–CO angle, the structure being nearly identical to those of **4** and **5**.

The tantalum alkyl complex $[Ta(CO)_2(dmpe)_2Me]$ (**7**) can be synthesized by reduction of $[Ta(CO)_2(dmpe)_2Cl]$ to form the highly reduced Ta(–I) species $Na[Ta(CO)_2(dmpe)_2]$, followed by alkylation with MeI or MeOTf.[33] In a similar manner, alkylation of $Na[V(CO)_2(dmpe)_2]$ with MeOTf yields the new complex $[V(CO)_2(dmpe)_2Me]$ (**8**), contaminated with substantial amounts of *trans*-$[V(CO)_2(dmpe)_2]$. Formation of the latter 17-electron species is presumably a result of competing alkylation and electron-transfer reactions. In a similar manner, reaction of

(59) Coffindaffer, T. W.; Steffy, B. D.; Rothwell, I. P.; Folting, K.; Huffman, J. C.; Streib, W. E. *J. Am. Chem. Soc.* **1989**, *111*, 4742.
(60) Felten, C.; Richter, J.; Priebsch, W.; Rehder, D. *Chem. Ber.* **1989**, *122*, 1617.

Table VI. Selected Bond Lengths (Å) and Angles (deg) for $[Ta(CO)_2(depe)_2Cl]$ (**6**)[a]

	Bond Lengths		
Ta–P1	2.5906 (7)	Ta–P2	2.5729 (7)
Ta–P3	2.6312 (8)	Ta–P4	2.6082 (8)
Ta–Cl	2.021 (3)	Ta–C2	2.008 (3)
C1–O1	1.168 (4)	C2–O2	1.184 (4)
Ta–Cl	2.5900 (8)		
	Bond Angles		
P1–Ta–P2	73.39 (2)	P4–Ta–C2	117.04 (9)
P2–Ta–P3	162.34 (2)	P2–Ta–C1	78.66 (2)
P1–Ta–C1	116.55 (9)	C1–Ta–Cl	142.92 (9)
P2–Ta–C2	117.01 (9)	Ta–C2–O2	179.3 (3)
P4–Ta–C1	80.48 (9)	P1–Ta–P4	161.55 (2)
P1–Ta–C1	82.96 (2)	P3–Ta–P4	74.46 (2)
P4–Ta–C1	78.83 (2)	P2–Ta–C1	77.72 (9)
Ta–C1–O1	177.3 (3)	P3–Ta–C2	76.99 (8)
P1–Ta–P3	100.87 (2)	C1–Ta–C2	66.9 (1)
P2–Ta–P4	105.55 (2)	P3–Ta–C1	84.11 (2)
P1–Ta–C2	78.23 (9)	C2–Ta–C1	150.13 (9)
P3–Ta–C1	119.17 (9)		

bond types	min	max	mean
P-CH_3	1.833 (3)	1.848 (3)	1.841
P-CH_2	1.835 (3)	1.862 (3)	1.844
CH_2-CH_2	1.523 (5)	1.527 (5)	1.525
CH_2-CH_3	1.518 (5)	1.532 (5)	1.525

[a] See Figure 5 for atom-labeling scheme. Standard deviations in the last significant figure(s) are given in parentheses.

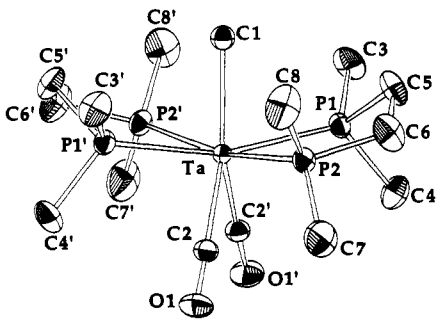

Figure 6. ORTEP view of $[Ta(CO)_2(dmpe)_2Me]$ (**7**), showing 30% thermal ellipsoids.

$Na[V(CO)_2(dmpe)_2]$ with 1 equiv of R_3SiX reagents gives a mixture of *trans*-$[V(CO)_2(dmpe)_2]$ and the siloxycarbyne $[V(COSiR_3)(CO)(dmpe)_2]$.[10]

The ^1H NMR spectra of **7** and **8** display upfield quintets at −1.52 (J_{PH} = 11 Hz) and −1.80 ppm (J_{PH} = 12 Hz), respectively, diagnostic for the σ-alkyl ligand. The $^{31}P\{^1H\}$ NMR spectrum of **8** shows a broad signal centered at 64 ppm (quadrupolar coupling to ^{51}V, $I = {}^7/_2$, 100%, not resolved). In a series of structurally related $[V(CO)_2(dmpe)_2X]$ complexes (X = Cl, CF_3CO_2, $MeCO_2$, $EtCO_2$, N_3, CN, $PhHPO_2$, and NH_2SO_3), the ^{31}P chemical shifts were found to occur in the range 52.6–57.4 ppm.[36]

X-ray structure determinations were carried out on compounds **7** and **8**, and the resulting ORTEP diagrams are displayed in Figures 6 and 7, respectively. Important bond distances and angles are listed in Tables VII and VIII. A capped trigonal prismatic geometry is found for both of these alkyl complexes, as was the case for the halide derivatives. The bond lengths of 2.32 (1) and 2.31 (1) Å for the respective Ta–CH_3 and V–CH_3 bonds are the longest reported to date for either metal. This lengthening may be the result of high steric congestion at the metal center. Tantalum–carbon bond distances spanning the range 2.171 (7)–2.248 (28) Å are realized in several seven-coordinate Ta(V) complexes.[61-65] A slightly longer Ta–C bond length of 2.26 (1) Å occurs in $[CpMeTaC(Ph)C(Ph)C(Me)N^tBu]$.[66] W–C bond distances of 2.28 (1) and 2.29 (2) Å are reported for the seven-coordinate W(II) complexes $[W(CO)_2(PMe_3)_2(S_2CNMe_2)CH_3]$ and $[W(CO)_2(acac)(PMe_3)_2CH_3]$.[67,68] A longer M–C bond length would be expected for Ta(I) as compared to W(II), suggesting that the reduced oxidation state of the metal center in **7** and **8** is an important determinant of the long metal–carbon

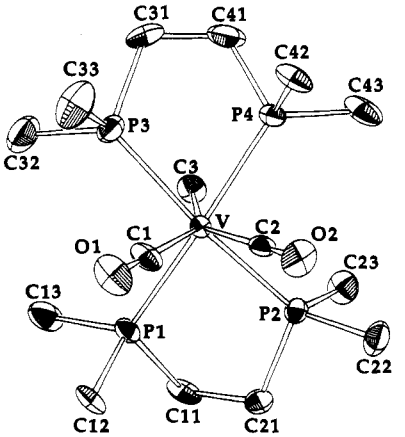

Figure 7. ORTEP view of $[V(CO)_2(dmpe)_2Me]$ (**8**), showing 40% thermal ellipsoids.

Table VII. Selected Bond Lengths (Å) and Bond Angles (deg) for $[Ta(CO)_2(dmpe)_2Me]$ (**7**)[a]

	Bond Lengths		
Ta–P1	2.553 (2)	Ta–P2	2.573 (2)
Ta–C1	2.32 (1)	Ta–C2	2.079 (7)
C2–O1	1.18 (1)		
	Bond Angles		
P1–Ta–P2	73.86 (6)	P2–Ta–C2	113.4 (2)
P1–Ta–P2′	104.38 (6)	Ta–C2–O1	178.8 (7)
P2–Ta–C1	84.55 (5)	P2–Ta–P2′	169.0 (1)
C2–Ta–C2′	66.6 (4)	P1–Ta–C2	118.1 (2)
P1–Ta–P1′	162.1 (1)	C1–Ta–C2	146.7 (2)
P1–Ta–C1	81.09 (5)		

bond types	min	max	mean
P-CH_3	1.80 (1)	1.83 (1)	1.82
P-CH_2	1.80 (1)	1.84 (1)	1.82
CH_2-CH_2	1.50 (1)	1.50 (1)	1.50

[a] See Figure 6 for atom-labeling scheme. Standard deviations in the last significant figure(s) are given in parentheses.

Table VIII. Selected Bond Lengths (Å) and Angles (deg) for $[V(CO)_2(dmpe)_2Me]$ (**8**)[a]

	Bond Lengths		
V–P1	2.456 (3)	V–P2	2.485 (3)
V–P3	2.432 (3)	V–P4	2.417 (3)
V–C1	1.88 (1)	V–C2	1.89 (1)
C1–O1	1.19 (1)	C2–O2	1.18 (1)
V–C3	2.31 (1)		
	Bond Angles		
P1–V–P2	76.8 (1)	P4–V–C2	77.9 (3)
P2–V–P3	161.9 (1)	P2–V–C3	82.4 (3)
P1–V–C1	77.5 (3)	C1–V–C3	144.5 (4)
P2–V–C2	77.0 (3)	V–C2–O2	178.2 (9)
P4–V–C1	118.4 (3)	P1–V–P4	162.4 (1)
P1–V–C3	81.4 (3)	P3–V–P4	74.7 (1)
P4–V–C3	81.0 (3)	P2–V–C1	119.3 (3)
V–C1–O1	178.2 (9)	P3–V–C2	117.3 (3)
P1–V–P3	103.6 (1)	C1–V–C2	67.9 (4)
P2–V–P4	99.4 (1)	P3–V–C3	79.8 (3)
P1–V–C2	117.2 (3)	C2–V–C3	147.6 (4)
P3–V–C1	77.8 (3)		

bond types	min	max	mean
P-CH_3	1.80 (1)	1.84 (1)	1.83
P-CH_2	1.82 (1)	1.87 (1)	1.85
CH_2-CH_2	1.51 (2)	1.51 (2)	1.51

[a] See Figure 7 for atom-labeling scheme. Standard deviations in the last significant figure(s) are given in parentheses.

Table IX. Comparison of C–M–C Angles and Carbonyl Stretching Frequencies for Selected Seven-Coordinate Group V and VI Complexes of the Form $[M(CO)_2(L\text{-}L)_2X]$ (L-L = Bidentate Chelating Ligand; X ≠ CO)[a]

compd	C–M–C angle, deg	ν_{CO}, cm^{-1}	ref
$[V(CO)_2(dmpe)_2O_2CEt]$	67.9 (7)	1808, 1750 (Nujol)	36
$[V(CO)_2(dmpe)_2MeCN]BPh_4$	68.7 (8)	1836, 1779 (Nujol)	36
$[V(CO)_2(dmpe)_2Me]$ (**8**)	67.9 (4)	1794, 1731 (Nujol)	*b*
$[Nb(CO)_2(dmpe)_2\{OAr\text{-}3,5\text{-}Me_2\}]$	66.7 (2)	1805, 1740 (Nujol)	59
$[Nb(CO)_2(dppe)_2Cl]$	56.7 (11)	1840, 1762 (toluene)	60
$[Nb(CO)_2(dmpe)_2Cl]$ (**4**)	69.1 (6), 69.4 (5)	1810, 1747 (Nujol)	*b*
$[Nb(CO)_2(dmpe)_2I]$ (**5**)	68.0 (4)		*b*
$[Ta(CO)_2(depe)_2Cl]$ (**6**)	66.9 (1)	1819, 1746 (Nujol)	*b*
$[Ta(CO)_2(dmpe)_2Me]$ (**7**)	66.6 (4)	1823, 1760 (THF)	*b*
$[Mo(CO)_2(dmpe)_2Cl]PF_6$	71.1 (2)	1945, 1880 (Nujol)	57
$[Mo(CO)_2(dppe)_2F]PF_6$	68.2 (6)	1945, 1889 (CH_2Cl_2)	*c*
$[Mo(CO)_2(diars)_2Cl]I_3 \cdot 2CHCl_3$	67.7 (24)	1960, 1888 (Nujol)[d]	*e*
$[Mo(CO)_2(S_2CNEt_2)(tht)]$	73.5 (5)		*f*
$[NEt_4][Mo(CO)_2(S_2CNEt_2)_2F]$	67.4 (3)	1884, 1797 (KBr)	*g*
$[W(CO)_2(dmpe)_2I]I$	74.6 (14), 70.1 (14)	1948, 1881 (CH_2Cl_2)	58
$[W(CO)_2(S_2CNEt_2)_2PPh_3]$[h]	71.6 (4), 71.7 (4)	1920, 1829 (Nujol)	*i*

[a] dmpe = 1,2-bis(dimethylphosphino)ethane, depe = 1,2-bis(diethylphosphino)ethane, dppe = 1,2-bis(diphenylphosphino)ethane. [b] This work. [c] Chandler, T.; Kriek, G. R.; Greenaway, A. M.; Enemark, J. H. *Cryst. Struct. Commun.* **1980**, *9*, 557. [d] Reported for I^- salt. [e] Drew, M. G. B.; Wilkins, J. D. *J. Chem. Soc., Dalton Trans.* **1973**, 2664. [f] Templeton, J. L.; Burgmayer, S. J. N. *Organometallics* **1982**, *1*, 1007. [g] Burgmayer, S. J. N.; Templeton, J. L. *Inorg. Chem.* **1985**, *24*, 2224. [h] Molecule adopts the 4:3 piano stool geometry. [i] Templeton, J. L.; Ward, B. C. *J. Am. Chem. Soc.* **1981**, *103*, 3743.

bond. The average Ta–P distance of 2.563 Å for **7** is somewhat shorter than the same distance in either **4** or **5**, perhaps indicating more metal-to-phosphorus π-back-bonding. The average Ta–CO distance of 2.079 Å is comparable to those found for **4** and **5**.

Comparisons for the vanadium–methyl bond distance in **8** are harder to make. The longest previously reported V–C bond is 2.219 (4) Å, occurring in [CpVMe(dmpe)].[69,70] The average V–P distance of 2.448 Å can be compared to the same distances in $[V(CO)_2(dmpe)_2O_2CEt]$ (average V–P = 2.486 Å) and $[V(CO)_2(dmpe)_2MeCN]BPh_4$ (average V–P = 2.472 Å).[36] Similarly, the V–CO distance in **8** (average V–CO = 1.885 Å) is slightly longer than that found in $[V(CO)_2(dmpe)_2O_2CEt]$ (average V–CO = 1.856 Å) and $[V(CO)_2(dmpe)_2MeCN]BPh_4$ (average V–CO = 1.841 Å).

The structures of **4–8** all adopt capped trigonal prismatic (CTP) geometries, with the X ligand occupying the capping position, four phosphorus atoms forming the capped quadrilateral face, and the two carbonyl ligands occupying the unique edge. A similar geometry is observed for the related $[M(CO)(CNR)(dmpe)_2Cl]$ (M = Nb, Ta; R = ^{t}Bu, Cy, Et) and $[Ta(CNMe)_2(dmpe)_2Cl]$ complexes.[55] Table IX lists structurally characterized $[M(CO)_2(L\text{-}L)_2X]$ (L-L is chelating ligand, X ≠ CO) complexes of group V and VI. For all but one of the listed structures a CTP geometry is adopted. The infrared stretching frequencies for the compounds listed in Table IX span the range 1960–1731 cm^{-1} for the terminal CO ligands, indicative of the low-valent nature of the complexes. The group V complexes show lower ν_{CO} values than the group VI compounds. In addition, close nonbonded distances and small angles between the CO ligands are found, possible factors which can lead to reductive coupling of two CO ligands.[9]

Summary. A high-yield (94%) synthesis of $[Ta(CO)_2(dmpe)_2Cl]$ has been obtained. The $[M(CO)_2(L\text{-}L)_2X]$ complexes (L-L = dmpe, depe; X = halide) are important precursor molecules for the reductive coupling CO ligands and the synthesis of mixed isocyanide/CO complexes of the type $[M(CO)(CNR)(dmpe)_2X]$, which afford the mixed coupling of CO and CNR.[55] In addition, they are starting materials for the preparation of metal alkyls of the type $[M(CO)_2(dmpe)_2Me]$ (M = V or Ta), which have been structurally characterized in this work. During our search for an optimal route to $[Ta(CO)_2(dmpe)_2Cl]$, the novel anthracene complex $[Ta(\eta^4\text{-anthracene})(dmpe)_2Cl]$ was prepared and structurally characterized, and the structure of $[TaCl_2(dmpe)_2]$ was also determined.

Acknowledgment. This work was supported by a grant from the National Science Foundation. We thank Dr. A. Stanger for a preprint of ref 54.

Supplementary Material Available: For **1**, **2**, and **4–8**, Tables S1–S3, S5–S7, S9, S10, S12–S14, S16, S17, S19, S20, S22, and S23, listing atomic coordinates and thermal parameters (25 pages). Ordering information is given on any current masthead page.

(61) Chisholm, M. H.; Tan, L.-S.; Huffman, J. C. *J. Am. Chem. Soc.* **1982**, *104*, 4879.
(62) Wilkins, J. D.; Drew, M. G. B. *J. Organomet. Chem.* **1974**, *69*, 111.
(63) Drew, M. G. B.; Wilkins, J. D. *J. Chem. Soc., Dalton Trans.* **1974**, 1973.
(64) Drew, M. G. B.; Wilkins, J. D. *Acta. Crystallogr. Sect. B* **1975**, *31*, 2642.
(65) Drew, M. G. B.; Wilkins, J. D. *J. Chem. Soc., Dalton Trans.* **1973**, 1830.
(66) Curtis, M. D.; Real, J.; Hirpo, W.; Butler, W. M. *Organometallics* **1990**, *9*, 66.
(67) Carmona, E.; Contreras, L.; Poveda, M. L.; Sánchez, L. J.; Atwood, J. L.; Rogers, R. D. *Organometallics* **1991**, *10*, 61.
(68) Carmona, E.; Contreras, L.; Gutiérrez-Puebla, E.; Monge, A.; Sánchez, L. J. *Organometallics* **1991**, *10*, 71.
(69) Hessen, B.; Lemmen, T. H.; Luttikhedde, H. J. G.; Teuben, J. H.; Petersen, J. L.; Huffman, J. C.; Jagner, J.; Caulton, K. G. *Organometallics* **1987**, *6*, 2354.
(70) Holloway, C. E.; Melnfk, M. *J. Organomet. Chem.* **1986**, *304*, 41.